

# SCIENTIFIC REPORTS

OPEN

## An upper limit of Cr-doping level to Retain Zero-strain Characteristics of $\text{Li}_4\text{Ti}_5\text{O}_{12}$ Anode Material for Li-ion Batteries

Received: 10 July 2016

Accepted: 25 January 2017

Published: 24 February 2017

Hannah Song, Tae-Gyung Jeong, Su-Won Yun, Eun-Kyung Lee, Shin-Ae Park & Yong-Tae Kim

Since  $\text{Li}_4\text{Ti}_5\text{O}_{12}$  as a promising anode material in lithium-ion batteries (LIBs) has a poor rate performance due to low electronic conductivity, a doping of  $\text{Li}_4\text{Ti}_5\text{O}_{12}$  with heterogeneous atoms has been considered to overcome this problem. Herein, we report that there is an upper limit of doping level to maintain the zero strain characteristics of  $\text{Li}_4\text{Ti}_5\text{O}_{12}$  lattice during charge/discharge process. By using synchrotron studies, it was revealed that the  $\text{Li}^+$  diffusivity was maximized at a certain doping level for which the conductivity was markedly increased with maintaining the zero strain characteristics. However, with more doses of dopants over the upper limit, the lattice shrank and therefore the  $\text{Li}^+$  diffusivity decreased, although the electronic conductivity was further increased in comparison with the optimal doping level.

Lithium-ion batteries are a commercial success, but there are safety concerns about the carbon-based negative-electrode materials used in them<sup>1,2</sup>. Because their operating potential is relatively low and close to that of lithium metal, dendrites form on the surface of the carbon-based negative electrodes causing a short circuit, especially at high rates<sup>3,4</sup>. Cubic spinel  $\text{Li}_4\text{Ti}_5\text{O}_{12}$  has attracted much attention as a promising anode material for lithium-ion batteries because of its relatively high potential above 1.5 V (vs. Li), which imparts safety and stability to the battery. However, as an insulator,  $\text{Li}_4\text{Ti}_5\text{O}_{12}$  shows poor rate performance because of its low electronic and ionic conductivities<sup>5,6</sup>. To overcome this problem, doping a heterogeneous atom is an effective way to enhance the rate performance by changing the insulating characteristics<sup>7</sup>. Various transition metals such as Mg, Cr, Mn, Ta, Y, and Mo have been used as a dopant in  $\text{Li}_4\text{Ti}_5\text{O}_{12}$ , enhancing its rate performance<sup>3,8–15</sup>. Some have attributed the enhanced rate performance to the increased electronic conductivity upon doping. However, others have reported that enhanced electronic conductivity does not guarantee enhanced rate performance, probably because of the decrease in  $\text{Ti}^{4+}$ , which is the sole atom that participates in the redox reaction<sup>8,15</sup>. However, because only 40% of  $\text{Ti}^{4+}$  is reduced to  $\text{Ti}^{3+}$  in the charge process ( $\text{Li}_4\text{Ti}_5\text{O}_{12} \rightarrow \text{Li}_7\text{Ti}_5\text{O}_{12}$ ), some other factor must affect the rate performance of  $\text{Li}_4\text{Ti}_5\text{O}_{12}$ . Lithium-ion diffusivity and electronic conductivity are the main factors that play a role in high rate performance, and many researchers have tried to synthesize nanoscale particles into various shapes to shorten the lithium-ion pathways<sup>16–18</sup>.

Under doping of a heterogeneous atoms, changes in the lattice structures in  $\text{Li}_4\text{Ti}_5\text{O}_{12}$  can occur because bond lengths or bonding symmetry can change around the heterogeneous dopant. Those structural changes could affect the diffusion rate of lithium ions into the lattice. We studied how those structural changes affect the lithium-ion diffusivity and rate capability of  $\text{Li}_4\text{Ti}_5\text{O}_{12}$ . Then, we found a lattice structure requirement needed for the zero-strain  $\text{Li}_4\text{Ti}_5\text{O}_{12}$ .

### Results and Discussion

$\text{Cr}^{3+}$  is the dopant most used in  $\text{Li}_4\text{Ti}_5\text{O}_{12}$ , because its high octahedral site stabilization energy (OSSE) makes it possible to substitute it for 50% of the atoms positioned at 16d sites<sup>9,19</sup>. In a manner similar to that used in our previous studies, we prepared  $\text{Li}_{4-x/3}\text{Ti}_{5-2x/3}\text{Cr}_x\text{O}_{12}$  ( $x = 0, 1, 2, 3$ ) by replacing one lithium ion and two titanium ions at the octahedral sites with three chromium ions ( $\text{Li}^{++} + 2\text{Ti}^{4+} \rightarrow 3\text{Cr}^{3+}$ ). Figure 1a presents the X-ray diffraction (XRD) patterns of the synthesized samples. All the patterns match well with the cubic spinel structure without any side peaks. When the amount of the dopant  $\text{Cr}^{3+}$  increased, a significant change in the lattice structure was

Department of Energy Systems, Pusan National University, Busan 609-735, Republic of Korea. Correspondence and requests for materials should be addressed to Y.-T.K. (email: yongtae@pusan.ac.kr)

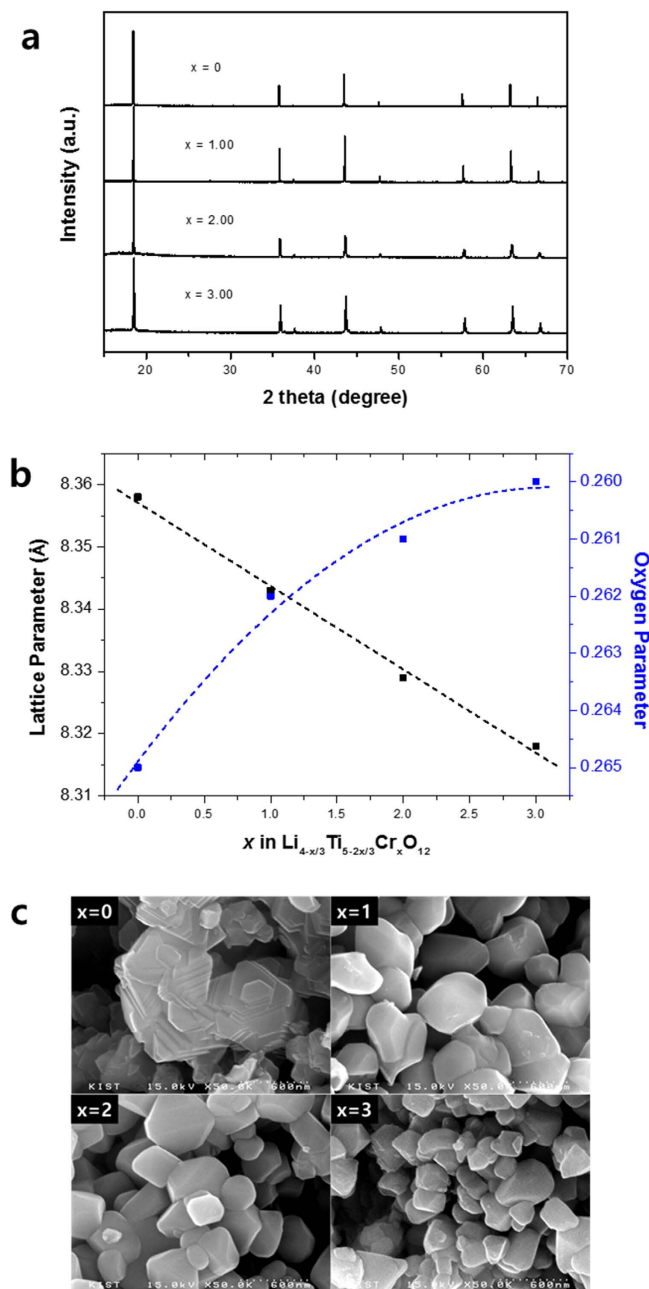


**Figure 1.** (a) XRD patterns (b) lattice parameters and oxygen parameters, and (c) SEM images of  $\text{Li}_{4-x/3}\text{Ti}_{5-2x/3}\text{Cr}_x\text{O}_{12}$  ( $x=0, 1, 2, 3$ ).

observed using Rietveld refinement. Figure 1b presents the lattice parameter of  $\text{Li}_4\text{Ti}_{5-2x}\text{Cr}_x\text{O}_{12}$ , which decreased linearly as the doping amount increased. This was expected because the average ionic radii at  $16d$  octahedral sites decreased when one  $\text{Li}^+$  (0.76 Å) and two  $\text{Ti}^{4+}$  (0.61 Å) were replaced by three  $\text{Cr}^{3+}$  (0.62 Å). Figure 1b also shows the variation in the fractional coefficient of oxygen ions in the lattice. In general, the oxygen parameter decreased when near 0.25, which is the ideal value for oxygen ions. The results imply that distortion of the lattice structure decreased with an increase in the doping amount of  $\text{Cr}^{3+}$ .

Electronic conductivity of the synthesized samples was measured using the van der Pauw method. A coin type pellet of active materials was fabricated by using the laboratory hydraulic press with the maximum pressure of 25 ton. Au paste was used to form the electrode at the position of cardinal points and Au wire was used to connect the measurement port of Hall effect measurement system. The electronic conductivity of bare  $\text{Li}_4\text{Ti}_5\text{O}_{12}$  could not be measured because it was extremely low ( $<10^{-13}$  S/cm) and out of measurement range. As seen in Fig. 2, the electronic conductivity of  $\text{Li}_4\text{Ti}_5\text{O}_{12}$  increased to about  $10^{-7}$  S/cm under doping with  $\text{Cr}^{3+}$ ; this is six orders of magnitude greater than that of bare  $\text{Li}_4\text{Ti}_5\text{O}_{12}$ . The electronic conductivity was markedly enhanced with the increase of doping level, because the carrier density was increased by the extra electrons donated by  $\text{Cr}^{3+}$  (Fig. 2).

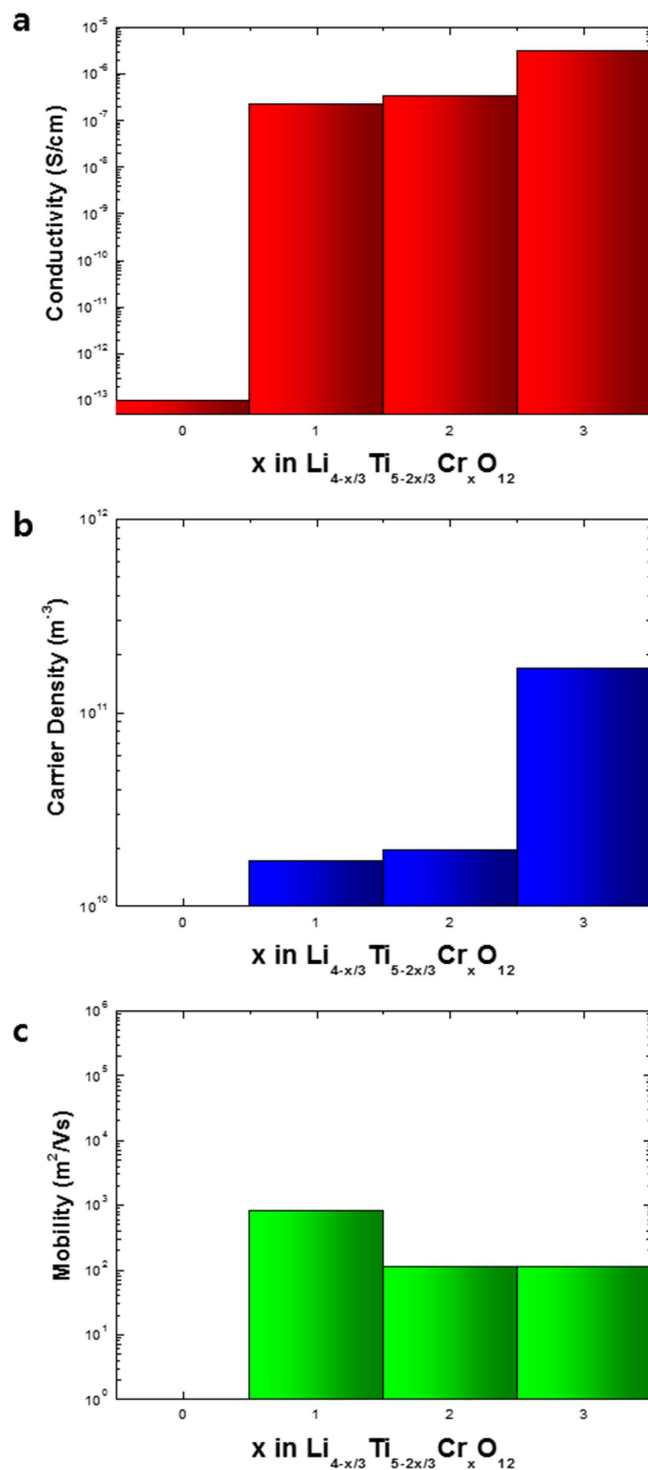


**Figure 2.** Electronic conductivity, Carrier density and Mobility of  $\text{Li}_{4-x/3}\text{Ti}_{5-2x/3}\text{Cr}_x\text{O}_{12}$  ( $x = 0, 1, 2, 3$ ).

In general, the enhanced electronic conductivity results in enhanced rate performance of  $\text{Li}_4\text{Ti}_5\text{O}_{12}$ . To understand the effect of doping on electrochemical performance, we performed battery tests at various C-rates. Figure 3a shows representative charge–discharge curves for all samples at 0.5 C. The voltage difference between the charge and discharge curves decreased with  $\text{Cr}^{3+}$  doping, indicating that the voltage polarization decreased upon doping. However, the polarization increased with the  $\text{Cr}^{3+}$  doping level over  $x = 1$ . The specific capacity of each sample was inversely proportional to the voltage difference between the charge and discharge curves. Figure 3b shows the rate capability of all samples. The  $\text{Li}_{4-x/3}\text{Ti}_{5-2x/3}\text{Cr}_x\text{O}_{12}$  ( $x = 1$ ) had the highest rate capability because it had the smallest voltage difference between the charge and discharge curves. Also, the  $\text{Li}_{4-x/3}\text{Ti}_{5-2x/3}\text{Cr}_x\text{O}_{12}$  ( $x = 1$ ) exhibited good cycle performance at 1 C in Fig. S2. However, Fig. 3b and c show that the rate capability decreased with increasing the doping level of  $\text{Cr}^{3+}$  over  $x = 1$  despite the increased electronic conductivity. Therefore, using

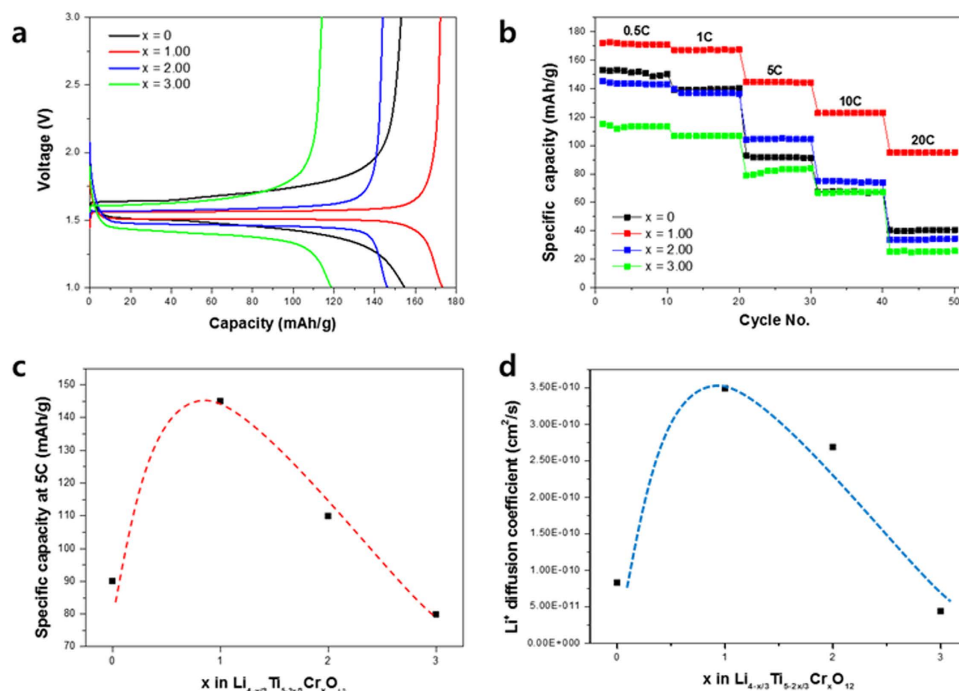


**Figure 3.** (a) Charge–discharge curves at 0.5C (b) rate capability (c) specific capacity at 5 C, and (d)  $\text{Li}^+$  diffusivity of  $\text{Li}_{4-x/3}\text{Ti}_{5-2x/3}\text{Cr}_x\text{O}_{12}$  ( $x = 0, 1, 2, 3$ ).

the galvanostatic intermittent titration technique (GITT), we measured  $\text{Li}^+$  diffusivity, which is one of the main factors that affect the rate capability. Figure 3d shows the  $\text{Li}^+$  diffusivity of  $\text{Li}_{4-x/3}\text{Ti}_{5-2x/3}\text{Cr}_x\text{O}_{12}$  with increasing doping amount of  $\text{Cr}^{3+}$ . While the electronic conductivity increased linearly in Fig. 2, the  $\text{Li}^+$  diffusivity showed a volcano-type variation, with a peak at  $x = 1$  for  $\text{Li}_{4-x/3}\text{Ti}_{5-2x/3}\text{Cr}_x\text{O}_{12}$ , and decreased linearly when the doping amount was greater than  $x = 1$ , which is similar to the variation of specific capacity at a high C-rate seen in Fig. 3c. This result implies that  $\text{Li}^+$  diffusivity more than electronic conductivity affects the rate capability with a linear increase. The highest  $\text{Li}^+$  diffusivity occurs when  $x = 1$  because of the decrease in structural disorder caused by the swing of oxygen ions in the lattice. However, when the doping amount of  $\text{Cr}^{3+}$  was increased over  $x = 1$ , the  $\text{Li}^+$  diffusivity linearly decreased despite the increased structural order.

To understand the volcano-type variation of the  $\text{Li}^+$  diffusivity, the particle size of all synthesized samples was observed using scanning electron microscopy (SEM) (Fig. 1c). The particle size generally decreased when the doping amount increased, which did not seem to affect the volcano-type variation of  $\text{Li}^+$  diffusivity. Also, Cr ions in the powder were evenly distributed as shown in Fig. S1. Therefore, we carried out *in situ* XRD measurements of all samples to identify changes to the lattice structure when  $\text{Li}^+$  is inserted into the lattice. Figure 4b shows changes in the lattice dimension as a function of  $y$  in  $\text{Li}_{4-x/3+3y}\text{Ti}_{5-2x/3}\text{Cr}_x\text{O}_{12}$  (the *in situ* XRD patterns of each sample are shown in Fig. 5). For samples of  $\text{Li}_{4-x/3}\text{Ti}_{5-2x/3}\text{Cr}_x\text{O}_{12}$  when  $x = 0$  and  $x = 1$ , there was no significant change in the lattice dimension when  $\text{Li}^+$  was inserted, which is the zero-strain characteristic of the cubic spinel  $\text{Li}_4\text{Ti}_5\text{O}_{12}$ . The lattice dimensions of the anode materials in lithium-ion batteries usually expand because of the change in ionic radii of the redox species in a solid matrix. However, during the lithiation of  $\text{Li}_4\text{Ti}_5\text{O}_{12}$ , the oxygen ions in the lattice of  $\text{Li}_4\text{Ti}_5\text{O}_{12}$  swing to their ideal positions, leading to its rock salt structure without distortion from the distorted spinel structure as shown in Fig. 4a. That is why  $\text{Li}_4\text{Ti}_5\text{O}_{12}$  has zero strain although the Ti–O bond length increases during lithiation<sup>20</sup>. However, zero strain was not maintained when  $x = 2$  and  $x = 3$ . Figure 4b shows the significant change in the lattice dimension for the two samples during lithiation. When the doping amount of  $\text{Cr}^{3+}$  increased, the lattice dimensions expanded as the lithium ions were inserted into the lattice. The lattice of the  $\text{Li}_{4-x/3}\text{Ti}_{5-2x/3}\text{Cr}_x\text{O}_{12}$  ( $x = 2$ ) sample expanded from 8.329 to 8.339(1) Å, and the lattice of the  $\text{Li}_{4-x/3}\text{Ti}_{5-2x/3}\text{Cr}_x\text{O}_{12}$  ( $x = 3$ ) sample expanded from 8.318 to 8.340(1) Å. Rapid changes in the lattice dimensions of the two samples were observed at the beginning of lithiation. These changes in lattice structure could have been caused by the decrease in lattice parameter that occurs with an increase in the doping amount of  $\text{Cr}^{3+}$ . If the lattice parameter of the doped  $\text{Li}_4\text{Ti}_5\text{O}_{12}$  is less than about 8.34 Å, the lattice dimension will expand to about 8.34 Å during lithiation. Thus, the zero-strain characteristics of  $\text{Li}_4\text{Ti}_5\text{O}_{12}$  is retained when the lattice parameter is larger than a specific size, and if the doped  $\text{Li}_4\text{Ti}_5\text{O}_{12}$  loses the zero-strain characteristic because of a smaller lattice parameter, the  $\text{Li}^+$  diffusivity would decrease, resulting in the deterioration of electrochemical performance. Therefore, the changes in the lattice structure and the improvement in electronic conductivity upon doping should enhance the electrochemical performance of  $\text{Li}_4\text{Ti}_5\text{O}_{12}$ .

In conclusion, we studied how the changes in the lattice structure of  $\text{Li}_4\text{Ti}_5\text{O}_{12}$  upon doping a heterogeneous atom affect its electrochemical properties. Unless the lattice parameter is larger than a specific size after doping,  $\text{Li}_4\text{Ti}_5\text{O}_{12}$  would lose its zero-strain characteristic because the lattice dimensions would expand during lithiation.

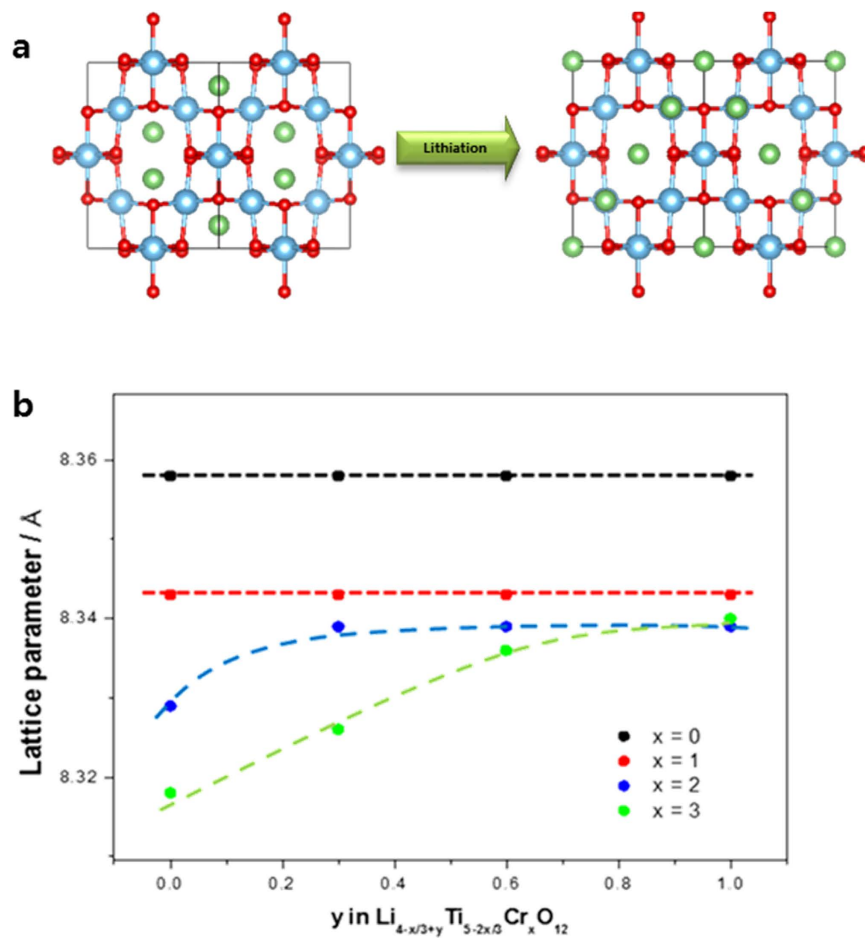


**Figure 4.** (a) Lattice structural changes of  $\text{Li}_4\text{Ti}_5\text{O}_{12}$  anode materials during lithiation showing the zero-strain characteristic of them. (b) Changes in the lattice dimension of  $\text{Li}_{4-x/3+y}\text{Ti}_{5-2x/3}\text{Cr}_x\text{O}_{12}$  as a function of  $y$ .

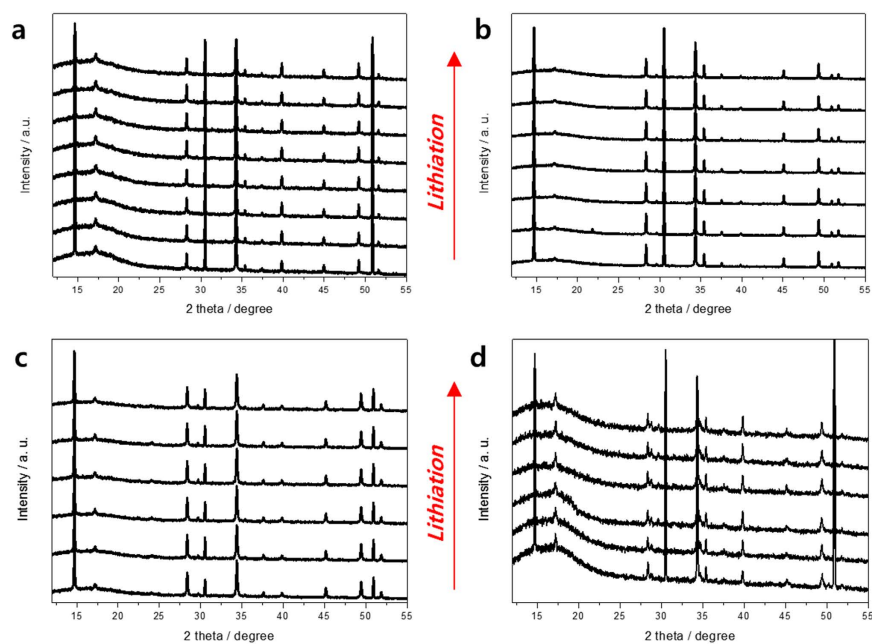


**Figure 5.** *In-situ* XRD patterns of  $\text{Li}_{4-x/3}\text{Ti}_{5-2x/3}\text{Cr}_x\text{O}_{12}$  (a)  $x = 0$  (b)  $x = 1$  (c)  $x = 2$ , and (d)  $x = 3$  during lithiation process.

Those structural changes cause the deterioration of the diffusion of lithium ions into the lattice, which results in the deterioration of rate capability. Therefore, to design  $\text{Li}_4\text{Ti}_5\text{O}_{12}$  with a high rate capability by doping a heterogeneous atom, the kind of dopant and the amount of doping should be controlled keeping in mind the changes in the lattice structure that occur.

## Methods

**Synthesis.**  $\text{Li}_{4-x/3}\text{Ti}_{5-2x/3}\text{Cr}_x\text{O}_{12}$  ( $x=0, 1, 2, 3$ ) was synthesized by dissolving  $\text{LiOH}\cdot\text{H}_2\text{O}$  in water and adding  $\text{TiO}_2$  and  $\text{Cr}(\text{NO}_3)_3\cdot 9\text{H}_2\text{O}$  to the solution with the appropriate molar ratios. After ball-milling for 2 h at 50 Hz, the solution was evaporated and dried in a vacuum oven at  $80^\circ\text{C}$  for 24 h. Then, the ground powder was annealed at  $800^\circ\text{C}$  for 12 h in air at a heating rate of  $5^\circ\text{C}/\text{min}$ .

**Characterization.** Electrochemical tests were performed using 2032 coin cells assembled with working electrodes coated on Cu foil at a mass ratio of active material:acetylene black:PVDF of 80:10:10 and reference/counter electrodes made of Li metal on a Cu mesh. The mass loading of active material was about  $0.06 \sim 0.062 \text{ mg}/\text{mm}^2$ .  $\text{LiPF}_6$  (1 M) in ethylene carbonate and dimethyl carbonate (DMC) (1:1 v/v) were used as the electrolyte. A polypropylene membrane was used as a separator. The coin cells were assembled in a glove box filled with Ar gas, and all electrochemical tests were carried out using a battery cycler (WC3000S, WonATech) at different C-rates in the voltage range of 1.0–3.0 V (vs. Li). The diffusion coefficients of the Li ions in all samples were measured using GITT with current application of  $30 \text{ s}^{21}$ . High-resolution powder diffraction and *in situ* XRD patterns of the synthesized powders were measured with the 9B HRPD and 3D X-ray scattering (XRS) beamlines at the Pohang Light Source (PLS) with a wavelength of 1.5495 and 1.24 Å, respectively.

## References

1. Arico, A. S., Bruce, P., Scrosati, B., Tarascon, J.-M. & van Schalkwijk, W. Nanostructured materials for advanced energy conversion and storage devices. *Nat. Mater.* **4**, 366–377 (2005).
2. Mahmoud, A., Amarilla, J. M., Lasri, K. & Saadoun, I. Influence of the synthesis method on the electrochemical properties of the  $\text{Li}_4\text{Ti}_5\text{O}_{12}$  spinel in li-half and li-ion full-cells. A systematic comparison. *Electrochim. Acta* **93**, 163–172 (2013).
3. Guo, M., Wang, S., Ding, L.-X., Huang, C. & Wang, H. Tantalum-doped lithium titanate with enhanced performance for lithium-ion batteries. *J. Power Sources* **283**, 372–380 (2015).
4. Ding, Y., Li, G. R., Xiao, C. W. & Gao, X. P. Insight into effects of graphene in  $\text{Li}_4\text{Ti}_5\text{O}_{12}$ /carbon composite with high rate capability as anode materials for lithium ion batteries. *Electrochim. Acta* **102**, 282–289 (2013).
5. Li, N., Liang, J., Wei, D., Zhu, Y. & Qian, Y. Solvothermal synthesis of micro-/nanoscale  $\text{Cu}/\text{Li}_4\text{Ti}_5\text{O}_{12}$  composites for high rate li-ion batteries. *Electrochim. Acta* **123**, 346–352 (2014).
6. Zhao, Z., Xu, Y., Ji, M. & Zhang, H. Synthesis and electrochemical performance of f-doped  $\text{Li}_4\text{Ti}_5\text{O}_{12}$  for lithium-ion batteries. *Electrochim. Acta* **109**, 645–650 (2013).
7. Song, H. & Kim, Y.-T. A mo-doped  $\text{tinb}_2\text{O}_7$  anode for lithium-ion batteries with high rate capability due to charge redistribution. *Chem. Commun.* **51**, 9849–9852 (2015).
8. Chen, C. H. *et al.* Studies of mg-substituted  $\text{Li}_{4-x}\text{Mg}_x\text{Ti}_5\text{O}_{12}$  spinel electrodes ( $0 \leq x \leq 1$ ) for lithium batteries. *J. Electrochem. Soc.* **148**, A102–A104 (2001).
9. Ohzuku, T., Tatsumi, K., Matoba, N. & Sawai, K. Electrochemistry and structural chemistry of  $\text{Li}[\text{crti}]_4\text{O}_4$  (fd-3m) in nonaqueous lithium cells. *J. Electrochem. Soc.* **147**, 3592–3597 (2000).
10. Capsoni, D. *et al.* Cr and ni doping of  $\text{Li}_4\text{Ti}_5\text{O}_{12}$ : Cation distribution and functional properties. *J. Phys. Chem. C* **113**, 19664–19671 (2009).
11. Sun, Y.-K., Jung, D.-J., Lee, Y. S. & Nahm, K. S. Synthesis and electrochemical characterization of spinel  $\text{Li}[\text{Li}_{(1-x)/3}\text{Cr}_x\text{Ti}_{(5-2x)/3}]_4\text{O}_4$  anode materials. *J. Power Sources* **125**, 242–245 (2004).
12. Song, H. *et al.* Anomalous decrease in structural disorder due to charge redistribution in cr-doped  $\text{Li}_4\text{Ti}_5\text{O}_{12}$  negative-electrode materials for high-rate li-ion batteries. *Energy Environ. Sci.* **5**, 9903–9913 (2012).
13. Song, H. *et al.* Stabilization of oxygen-deficient structure for conducting  $\text{Li}_4\text{Ti}_5\text{O}_{12}$ -d by molybdenum doping in a reducing atmosphere. *Sci. Rep.* **4**, 4350–4357 (2014).
14. Capsoni, D. *et al.* Cations distribution and valence states in mn-substituted  $\text{Li}_4\text{Ti}_5\text{O}_{12}$  structure. *Chem. Mater.* **20**, 4291–4298 (2008).
15. Bai, Y.-J., Gong, C., Lun, N. & Qi, Y.-X. Yttrium-modified  $\text{Li}_4\text{Ti}_5\text{O}_{12}$  as an effective anode material for lithium ion batteries with outstanding long-term cyclability and rate capabilities. *J. Mater. Chem. A* **1**, 89–96 (2013).
16. Lee, S. C. *et al.* Spinel  $\text{Li}_4\text{Ti}_5\text{O}_{12}$  nanotubes for energy storage materials. *J. Phys. Chem. C* **113**, 18420–18423 (2009).
17. Wang, Y. *et al.* Synthesis and electrochemical performance of nano-sized  $\text{Li}_4\text{Ti}_5\text{O}_{12}$  with double surface modification of ti (iii) and carbon. *J. Mater. Chem.* **19**, 6789–6795 (2009).
18. Yu, S.-H. *et al.* Surfactant-free nonaqueous synthesis of lithium titanium oxide (lto) nanostructures for lithium ion battery applications. *J. Mater. Chem.* **21**, 806–810 (2011).
19. Ganesan, M.  $\text{Li}_4\text{Ti}_{2.5}\text{Cr}_{2.5}\text{O}_{12}$  as anode material for lithium battery. *Ionics* **14**, 395–401 (2008).
20. Ariyoshi, K., Yamato, R. & Ohzuku, T. Zero-strain insertion mechanism of  $\text{Li}[\text{Li}_{1/3}\text{Ti}_{5/3}]_4\text{O}_4$  for advanced lithium-ion (shuttlecock) batteries. *Electrochim. Acta* **51**, 1125–1129 (2005).
21. Weppner, W. & Huggins, R. A. Determination of the kinetic parameters of mixed-conducting electrodes and application to the system  $\text{Li}_3\text{sb}$ . *J. Electrochem. Soc.* **124**, 1569–1578 (1977).

## Acknowledgements

This work was supported by the National Research Foundation (NRF) of Korea grant (2015R1A2A1A10056156, GCRC-SOP), Nano-Convergence Foundation (R201500910), and Korea Institute of Energy Technology Evaluation and Planning (KETEP) grant (20153010041750).

## Author Contributions

H.S. and Y.-T.K. proposed the concept and H.S. performed the experiment. T.-G. Jeong, S.-W.Y., E.-K.L. and S.-A.P. participated in acquiring the data. H.S. and Y.-T.K. wrote the paper. All authors commented on the paper.

## Additional Information

**Supplementary information** accompanies this paper at <http://www.nature.com/srep>



**Competing financial interests:** The authors declare no competing financial interests.

**How to cite this article:** Song, H. *et al.* An upper limit of Cr-doping level to Retain Zero-strain Characteristics of  $\text{Li}_4\text{Ti}_5\text{O}_{12}$  Anode Material for Li-ion Batteries. *Sci. Rep.* 7, 43335; doi: 10.1038/srep43335 (2017).

**Publisher's note:** Springer Nature remains neutral with regard to jurisdictional claims in published maps and institutional affiliations.



This work is licensed under a Creative Commons Attribution 4.0 International License. The images or other third party material in this article are included in the article's Creative Commons license, unless indicated otherwise in the credit line; if the material is not included under the Creative Commons license, users will need to obtain permission from the license holder to reproduce the material. To view a copy of this license, visit <http://creativecommons.org/licenses/by/4.0/>

© The Author(s) 2017